Thermo-optic modulation of plasmonic bandgap on metallic photonic crystal slab

Fanghui Ren, Xiangyu Wang, and Alan X. Wang

Citation: Appl. Phys. Lett. **102**, 181101 (2013); doi: 10.1063/1.4804202
View online: http://dx.doi.org/10.1063/1.4804202
View Table of Contents: http://apl.aip.org/resource/1/APPLAB/v102/i18
Published by the American Institute of Physics.

Thermo-optic modulation of plasmonic bandgap on metallic photonic crystal slab

Fanghui Ren, Xiangyu Wang, and Alan X. Wang[a)]
School of Electrical Engineering and Computer Science, Oregon State University, Corvallis, Oregon 97331, USA

(Received 11 January 2013; accepted 21 April 2013; published online 6 May 2013)

We demonstrate active control of plasmonic bandgap on a metallic photonic crystal slab using thermo-optic effects. The Au grating, which is milled by focused-ion beam on a glass substrate, is designed to exhibit an extraordinary optical transmission and a sharp transitional edge for high modulation efficiency. Only a moderate refractive index modulation of $\Delta n = 0.0043$ is required to obtain more than 60% modulation depth with surface-normal optical coupling.
 [http://dx.doi.org/10.1063/1.4804202]

Periodic metallic structures with subwavelength features, which are usually referred as metallic photonic crystals, provide simultaneous electronic and photonic resonances in the same energy range, leading to highly unique properties such as extraordinary optical transmission (EOT),[1,2] photonic bandgap,[3] Fano resonances,[4,5] and nonlinear optical effects.[6] Compared with conventional surface-plasmon-polariton (SPP) waveguides formed by metal-dielectric thin films or stripes, metallic photonic crystals provide stronger optical mode confinement, smaller size, and better manipulation of incident photons. Although optical transmission of metallic photonic crystal slabs has been theoretically investigated[7,8] and experimentally characterized,[9] such plasmonic devices only find applications in optical sensors[10,11] employing the shift of the resonant frequency and the localized electric field to enhance light-matter interactions. Active control of plasmonic resonances on metallic photonic crystal slabs, which is indispensable for optical communication, is only achieved on exotic material systems such as metal-VO_2[12] and photo-addressable polymers,[13] which can provide a huge refractive index change ($\Delta n > 0.5$). Modulating plasmonic resonances with moderate index perturbation, although it has been implemented by long-range SPP waveguides,[14] remains to be a challenge on metallic photonic crystal slabs. Such attempt has been reported very recently,[15] however, demonstration of a working device is not successful.

In this paper, we present a theoretical design and experimental demonstration of a metallic photonic crystal slab, which consists of a gold (Au) grating with subwavelength slits on regular glass substrates. Unlike conventional SPP resonators with low quality-factor (Q-factor) Lorentzian resonant line-shapes due to the high Ohm-loss at optical frequencies, the discrete guided modes induced by Bragg-grating-modulated SPPs couple with the broadband Fabry-Perot (F-P) resonance in the narrow slits, resulting in strong asymmetric Fano resonances with sharp plasmonic bandgaps.[16] This unique design provides the possibility to actively control the optical transmission with moderate refractive index modulation that is achievable by thermo-optic or electro-optic effects.

The proposed structure consists of a one-dimensional (1-D) array of subwavelength slits perforated in an Au film, which is deposited on top of a Corning 1737 AMLCD glass substrate ($n = 1.5023$ at 1541 nm wavelength). The schematic illustration is shown in Figure 1(a). The geometric parameters of the metallic photonic crystal slab are shown in Figure 1(b) with the periodicity of p, the thickness of t, and the width of the slits as g. The glass substrate h is more than 1 mm and can be treated as infinite thick in our analysis. In real measurement, it will actually induce very weak F-P fringes. On metallic photonic crystal slabs, there are two possible Bragg-grating-modulated SPPs for surface-normally incident transverse-magnetic (TM) light: one at the air-Au surface, and the other at the Au-glass surface. As active control of the plasmonic device is based on thermo-optic effects of the glass substrate, we need to excite the Au-glass SPPs at 1.55 μm wavelength, which requires $p = 1.032\,\mu$m if we assume $n_{spp} = n_{glass}$. This is a good approximation if the frequency of the grating SPP is far from the plasmonic resonant frequency of Au. As the F-P resonance in the narrow slits has no cut-off frequency at long wavelength, design of the slit width g can be quite flexible. In our device, we choose $g = 100$ nm after considering the fabrication feasibility. The thickness of the Au grating determines the peak F-P resonant frequency, and thus it is critical to the total transmitted power. According to the analysis in Ref. 8, $t = 400$ nm leads to the strongest F-P resonance at 1.55 μm for a free standing Ag grating. Considering that the glass substrate will increase the effective refractive index, we design $t = 100$ nm to ensure that the aspect ratio of the slits is no more than 1 because patterning thicker metal film using focused-ion beam (FIB) is more challenging. The optical transmission in Figure 2(a) of the grating is simulated by DiffractMod of Rsoft^{TM}, which is based on Rigorous Coupled Wave Analysis (RCWA).[17] At the visible and near-infrared wavelength range from 400 nm to 2 μm, we can clearly observe the fundamental and high-order grating-modulated SPPs at both the Au-air and Au-glass surfaces, which show symbolic asymmetric Fano resonances. We also need to point out an interesting difference of the SPPs between the Au-glass and Au-air surfaces:

[a)]Author to whom correspondence should be addressed. Electronic mail: wang@eecs.oregonstate.edu

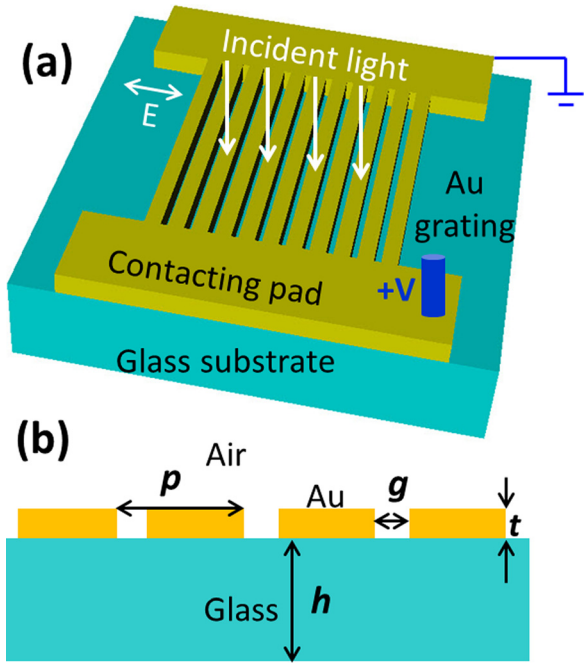

FIG. 1. (a) Schematic of the proposed metallic photonic crystal slab modulator, and (b) cross sectional view with geometrical parameters.

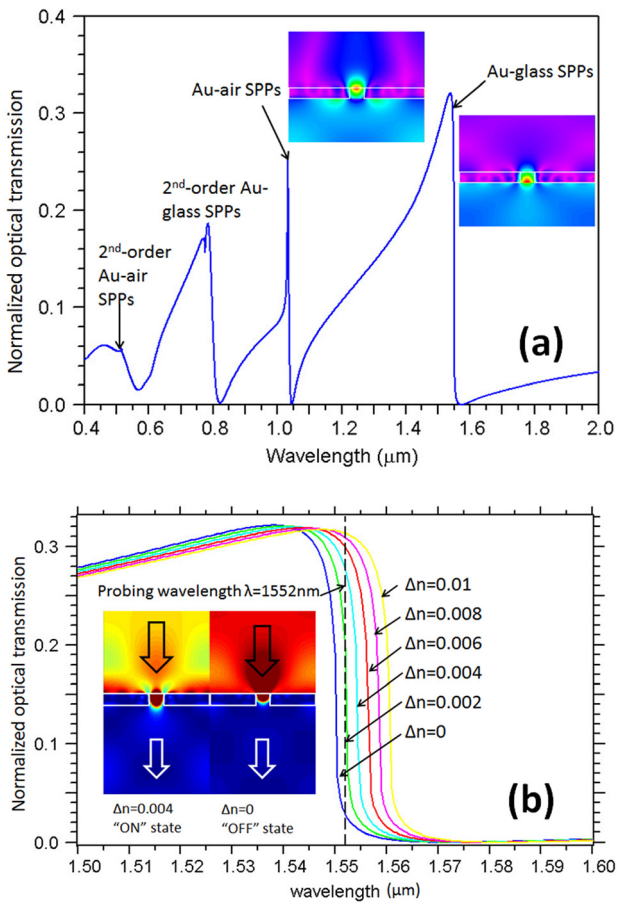

FIG. 2. (a) Simulated optical transmission of the metallic photonic crystal slab at visible and near-infrared wavelength; and (b) Simulated transmission spectra from 1.5–1.6 μm with different index modulation. The inset figure shows optical intensity distribution of the probing wavelength at 1552 nm at "ON" and "OFF" states.

the Q-factor of Au-air SPPs is much higher than that of the Au-glass SPPs, indicating a much longer photon lifetime, which is named as "ridge resonance" in Ref. 8. However, the sharp transitional edge of the low-Q Fano resonance at the Au-glass surface can still achieve efficient optical modulation, which is impossible on any conventional low-Q Lorentzian resonant structure. To verify this prediction, we simulate the optical transmission of the metallic photonic crystals with index modulation of the glass substrate from 0 to 0.01 at the wavelengths from 1.5 to 1.6 μm. Figure 2(b) proves that increasing the refractive index of the glass substrate red-shifts the transmission spectra. With a probing wavelength of 1552 nm, the simulated optical intensity distribution suggests that a slight index modulation of 0.004 is sufficient to cut off the resonant mode in the metal slits, achieving an effective optical modulation from 5% to 28%.

We started device fabrication by cleaning a $1'' \times 1''$ Corning 1737 AMLCD glass substrate with acetone, isopropyl alcohol (IPA), and de-ionized water. A 100 nm Au thin film was deposited by thermal evaporation with a deposition rate of 8 Å/s. The large size electrode pads were patterned by conventional contact photolithography followed by wet etching in gold etchant. After that, the 100 nm Au slits were etched by FIB (Quanta 3D, FEI Company), using a gallium ion current of 14.5 pA and a dose of 7 μC/cm^2. To achieve better accuracies of the metallic photonic crystal patterns, the integrated Nanometer Pattern Generation System (NPGS) in the FIB lithography is used to control the ion-gun, which can provide 0.5% error of the grating periodicity and 2% variation of the slit width.

Figure 3 shows the experimental setup for device characterization. The inset optical microscope and scanning electron microscopy (SEM) pictures show the fabricated metallic photonic crystal slab on top of the glass substrate. A broadband light source from 1.5–1.6 μm wavelength is coupled into a single-mode polarization-maintaining (PM) fiber with an in-line fiber polarizer, generating linearly polarized output light that is perpendicular to the grating direction (TM polarization with respect to the grating). The output light is then collimated by a 40× objective lens (NA = 0.65). The metallic photonic crystal sample is mounted on a three-dimensional translation/rotation stage, allowing precise spatial alignment and angular adjustment with respect to the collimated beam spot. The transmitted beam after the sample is focused by another 40× objective lens, which is then coupled into a standard SMF-28 fiber and measured by a HP 70951 A Optical Spectrum Analyzer. To actively control the optical transmission by thermo-optic effects, the Au contacting pads of the metallic photonic crystal slab are wire-bonded and connected with a DC power supply. A multi-meter is used to measure the current flowing through the device.

Figure 4 shows the EOT spectra of the metallic photonic crystal slab with normal incidence. A transitional edge is observed: the relative optical transmission drops from 90% to 40% within only 8 nm wavelength. This measurement qualitatively agrees with the simulated results shown in Figure 3, but the transitional edge is not as sharp as the numerical simulation, which is possibly caused by fabrication variation and imperfection of the collimated beam. A minimum transmission window, or plasmonic photonic bandgap, is observed

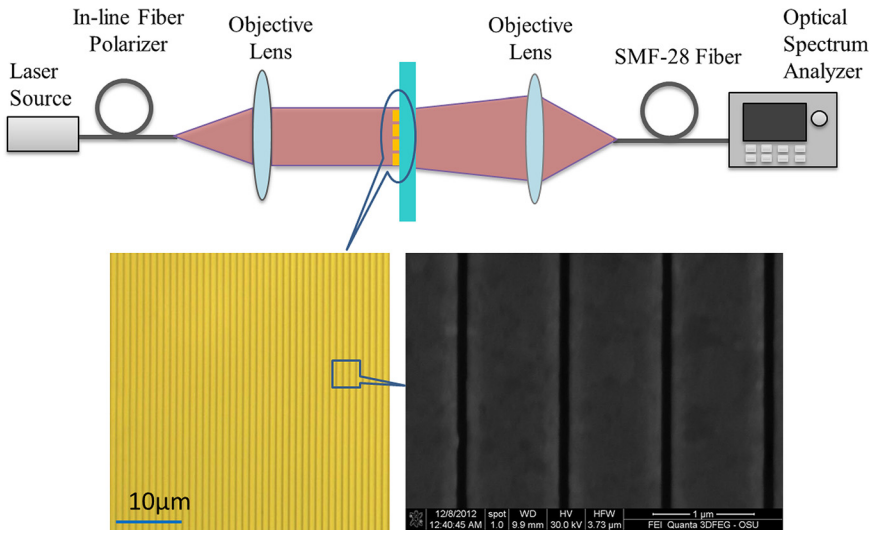

FIG. 3. Configuration of the experimental setup used for optical transmission measurement. The inset optical microscope and SEM pictures show the fabricated metallic photonic crystal slab.

beyond 1.57 μm, which also matches the numerical simulation. Figure 4 also shows the optical transmission spectra at 150 mA and 200 mA heating current, respectively. Since the refractive index of the glass substrate will increase when it is heated by the Au grating, a red-shift of the plasmonic resonance occurs, which can be explained by the zero-order relation,[18]

$$\lambda_0 = n_{spp} p, \tag{1}$$

$$\text{where} \quad n_{spp} = \text{Re}\left(\sqrt{\frac{\varepsilon_{Au}\varepsilon_d}{\varepsilon_{Au}+\varepsilon_d}}\right). \tag{2}$$

At 0 mA, $n_{spp} = 1.518$ is given by the dielectric constants of the glass $\varepsilon_d = 1.5023^2 = 2.257$, and the metal $\varepsilon_{Au} = -104.5 + 3.68i$ at 1550 nm,[19] which results in the SPP wavelength λ_0 at 1567 nm. By applying a current of 200 mA, a red-shift of 5 nm is attributed to the modulation of the refractive index of the glass substrate of $\Delta n = 0.0043$, which is calculated by Eqs. (1) and (2). This index modulation suggests that that the glass substrate was heated to ~540 °C if the thermo-optic coefficient is given as $dn/dT = 7.9 \times 10^{-6}$ °C.[20] To verify this estimation, we measured the total serial resistance between the two Au contacting pads to be 3.2 Ω by an Agilent 4155C semiconductor parameter analyzer with a Karlsuss PA-200 probe station. As the resistivity of thermally evaporated Au thin film is usually 3× as large as that of bulk Au ($\rho_{Au} = 2.2\ \mu\Omega$ cm),[21] the resistance of the photonic crystal slab region is determined to be about 0.74 Ω. With 200 mA heating current, the effective power dissipation of the plasmonic device is ~30 mW. Based on these parameters, a 2-D heat-transferring model simulated by Comsol 3.5a indicates that the glass substrate is heated to 595 °C. This 2-D heat-transferring simulation result is slightly higher than the previous calculation because it assumes that the heater is infinitely long in the third dimension. As we further increased the current to 220 mA, the Au grating was significantly overheated and some congregated clusters were observed in the SEM image in Figure 5, causing the failure of the device. The simulation and experimental data suggest that more efficient thermo-optic plasmonic devices should be built on silicon or polymer substrates that can provide much higher thermo-optic effects.

Thermal-optical modulation is also characterized on another equivalent plasmonic device using a probing wavelength at 1550 nm from a tunable laser. The transmitted signal is coupled to an InGaAs photodetector, and the photocurrent is monitored by a digital oscilloscope. The

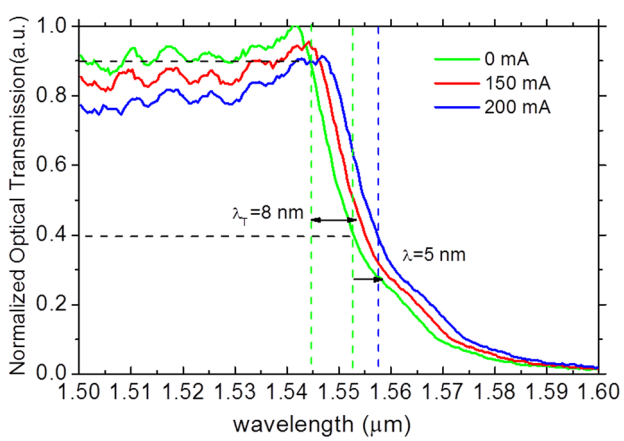

FIG. 4. Measured optical transmission spectra with different heating current.

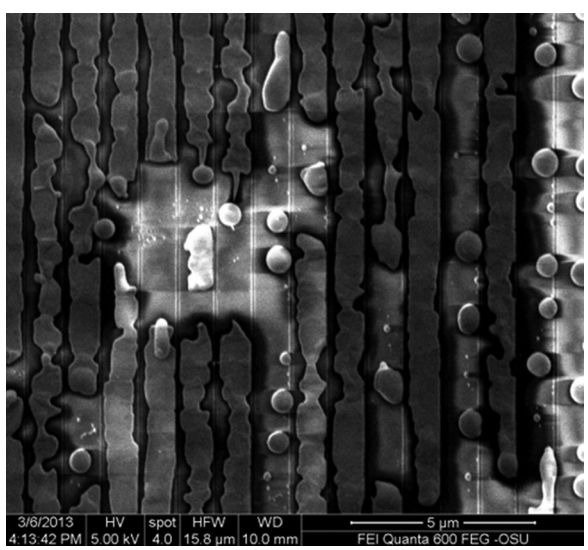

FIG. 5. SEM image of Au grating after applying 220 mA current, showing that the Au film aggregated into clusters.

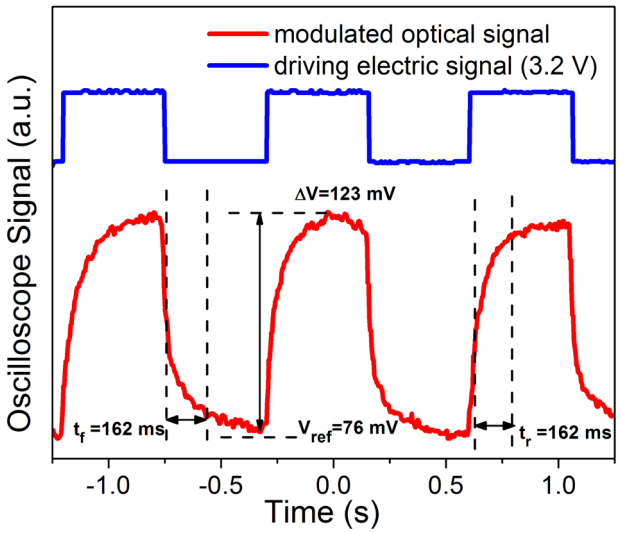

FIG. 6. Thermo-optic modulation of the plasmonic bandgap: the upper curve is the driving electric signal, and the lower curve is the responding optical signal.

device is driven by a square wave (0–3.2 V) from a function generator operating at 1.09 Hz, corresponding to heating currents from 0 to 200 mA. The electric driving signals and the corresponding optical signals are shown in Figure 6, with modulation depth (defined as the induced variation of the transmitted optical power normalized to the unperturbed optical output power) exceeding 60%. The rising time and falling time are measured to be 159 ms and 162 ms, respectively. This relatively low modulation speed is due to the slow thermal diffusion rate of the glass substrate.

In conclusion, we have demonstrated that the plasmonic bandgap of a metallic photonic crystal slab can be efficiently modulated by thermo-optic effects from a conventional glass substrate. This active control of plasmonic resonance is achieved by engineering the Fano resonance of the metallic photonic crystals to generate a sharp transitional edge. With only a moderate index modulation of 0.0043, we can achieve more than 60% modulation depth using surface-normal optical incidence. The power dissipation of the thermo-optic device is ~30 mW, which is majorly due to the small thermo-optic coefficient of the Corning glass substrate. We can still see that the sharpness of the transitional edge is not as perfect as that of the numerical simulation, which is possibly due to the fabrication variation and beam collimation. Further improvement to obtain an even sharper transitional edge will enable surface-normal electro-optic modulators using $LiNbO_3$ or nonlinear polymers[22] as the substrates for high-speed modulation with smaller index perturbation ($\Delta n \sim 0.001$). Such surface-normal plasmonic modulators can be easily expanded into arrayed structures. When integrated with vertical-surface emitting laser (VCSEL) array, it will provide enormous modulation bandwidth for board-level optical interconnects and millimeter-wave photonic systems.

This research is supported by the School of EECS at Oregon State University. The authors would like to thank Materials Synthesis and Characterization Facility (MASC), and Dr. Thomas K. Plant for the support in thin film evaporation and optical characterization.

[1]T. W. Ebbesen, H. J. Lezec, H. F. Ghaemi, T. Thio, and P. A. Wolff, Nature **391**, 667 (1998).
[2]J. A. Porto, F. J. Garcia-Vidal, and J. B. Pendry, Phys. Rev. Lett. **83**, 2845 (1999).
[3]J. G. Fleming, S. Y. Lin, I. El-Kady, R. Biswas, and K. M. Ho, Nature **417**, 52 (2002).
[4]B. Luk'yanchuk, N. I. Zheludev, S. A. Maier, N. J. Halas, P. Nordlander, H. Giessen, and C. T. Chong, Nature Mater. **9**, 707 (2010).
[5]A. Christ, SG Tikhodeev, N. A. Gippius, J. Kuhl, and H. Giessen, Phys. Rev. Lett. **91**, 183901 (2003).
[6]M. Kauranen and A. V. Zayats, Nat. Photonics **6**, 737 (2012).
[7]L. Martín-Moreno, F. J. García-Vidal, H. J. Lezec, K. M. Pellerin, T. Thio, J. B. Pendry, and T. W. Ebbesen, Phys. Rev. Lett. **86**, 1114 (2001).
[8]G. D'Aguanno, N. Mattiucci, M. J. Bloemer, D. de Ceglia, M. A. Vincenti, and A. Alù, J. Opt. Soc. Am. B **28**, 253 (2011).
[9]A. Christ, T. Zentgraf, J. Kuhl, S. G. Tikhodeev, N. A. Gippius, and H. Giessen, Phys. Rev. B **70**, 125113 (2004).
[10]D. Nau, A. Seidel, R. B. Orzekowsky, S. H. Lee, S. Deb, and H. Giessen, Opt. Lett. **35**, 3150 (2010).
[11]M. Grande, M. A. Vincenti, T. Stomeo, G. Morea, R. Marani, V. Marrocco, V. Petruzzelli, A. D'Orazio, R. Cingolani, and M. De Vittorio, Opt. Express **19**, 21385 (2011).
[12]J. Y. Suh, E. U. Donev, R. Lopez, L. C. Feldman, and R. F. Haglund, Appl. Phys. Lett. **88**, 133115 (2006).
[13]D. Nau, R. P. Bertram, K. Buse, T. Zentgraf, J. Kuhl, S. G. Tikhodeev, N. A. Gippius, and H. Giessen, Appl. Phys. B **82**, 543 (2006).
[14]T. Nikolajsen, K. Leosson, and S. I. Bozhevolnyi, Appl. Phys. Lett. **85**, 5833 (2004).
[15]J. Z. Xin, K. C. Hui, K. Wang, H. L. W. Chan, D. H. C. Ong, and C. W. Leung, Appl. Phys. A **107**, 101 (2012).
[16]D. De Ceglia, M. A. Vincenti, M. Scalora, N. Akozbek, and M. J. Bloemer, AIP Adv. **1**, 032151 (2011).
[17]M. G. Moharam and T. K. Gaylord, J. Opt. Soc. Am. **3**, 1780 (1986).
[18]H. Raether, *Surface Polaritions on Smooth and Rough Surfaces and on Gratings* (Springer-Verlag, Berlin, 1988).
[19]M. A. Ordal, L. L. Long, R. J. Bell, S. E. Bell, R. R. Bell, R. W. Alexander, and C. A. Ward, Appl. Opt. **22**, 1099 (1983).
[20]J. H. Wray and J. T. Neu, Opt. Soc. Am. **59**, 774 (1969).
[21]W. R. Veazey and C. D. Hodgman, *Handbook of Chemistry and Physics* (Chemical Rubber Pub. Co., 1919).
[22]H. Ma, A. K. Y. Jen, and L. R. Dalton, Adv. Mater. **14**, 1339 (2002).